View metadata, citation and similar papers at core.ac.uk
brought to you by CORE
provided by Tokushima University Institutional Repository

Vertically stacked graphene tunnel junction with structured water barrier

Jiyao Du*, Yukinobu Kimura, Masaaki Tahara, Kazushi Matsui, Hitoshi Teratani, Yasuhide Ohno, and Masao Nagase*

Graduate School of Advanced Technology and Science, Tokushima University, Minamijyosanjima 2-1, Tokushima 770-8506, Japan

E-mail: j_du@ee.tokushima-u.ac.jp E-mail: nagase@ee.tokushima-u.ac.jp

We report a vertically stacked graphene tunnel junction with an atomically thin insulating layer for novel function devices. The insulating water layer sandwiched between graphene samples as a tunnel barrier which is fabricated through deionized (DI) water treatment of epitaxial graphene. Two graphene samples fabricated by SiC thermal decomposition are directly bonded to each other in a face-to-face manner. Vertically stacked graphene samples without DI water treated formed an ohmic junction. By inserting the structured water layer as tunnel barrier, the stacked junction exhibits Direct tunneling (DT) characteristics in a low-electric-field regime and Fowler-Nordheim tunneling (FNT) characteristics in a high-electric-field regime. The thickness of the structured water layer is estimated to be 0.28 nm by fitting the FNT formula. The very thin structured water layer is stable as tunnel barrier on epitaxial graphene for diode devices, which will have a widely application in electronic devices.

1. Introduction

The excellent properties of graphene have stimulated much interest for applications in new generation novel functional electronic devices.[1-3] Recently, vertically stacked graphene junction systems have attracted much attention owing to their unique characteristics such as resonant tunneling and terahertz emission.[4-7] In tunnel junction, electrons are transported through a thin insulating barrier, from one electrode to the other. In stacked graphene junction, atomically thin two-dimensional materials such as hexagonal boron nitride (h-BN) and molybdenum disulfide (MoS_2) were utilized as tunneling barrier.[8-14] However, the fabrication processes of such reported devices are based on film-transfer technologies which are very complicated. Thus, simpler methods to construct stacked junction systems are desirable. In this paper, we demonstrate a simple fabrication technique to construct vertically stacked graphene tunneling junctions. Two samples of single-crystal graphene grown on a 4H-SiC(0001) substrate are directly bonded to each other in face-to-face manner. Before bonding, a thin water layer which acts as tunnel barrier is formed through deionized (DI) water treatment.[15] Through *I-V* measurement after fabricated, both direct tunneling (DT) and Fowler-Nordheim tunneling (FNT) phenomena are observed in the graphene/ water barrier/ graphene junction.

2. Experimental methods

2.1 Fabrication of graphene samples

The graphene samples were prepared using an infrared rapid thermal annealer (Thermo Riko SR-1800). The starting material was 4H-SiC (0001) semi-insulating substrate of size 10 mm × 10 mm, cut using the stealth-dicing technology. The substrate was subjected to thermal decomposition at 1660 °C in Ar environment (100 Torr) for five minutes, for the epitaxial graphene growth of sample A. Annealing was performed at 1640 °C for five minutes in Ar environment (100 Torr) to produce sample B. The quality of the samples were evaluated through Hall measurements, microscopic Raman spectroscopy

(Technospec uRaman532), and scanning probe microscopy (SPM; SPA400/Nanonavi SII-NT). The results of Hall effect measurements of sample A, before water treatment were 1590 Ω/□ in the sheet resistance, 744 cm^2/Vs in carrier mobility, and 5.48×10^{12} cm^{-2} in sheet carrier (electron) density, respectively. Those of sample B were 2360 Ω/□, 479 cm^2/Vs, and 6.04×10^{12} cm^{-2}, respectively. The results of microscopic Raman spectroscopy and SPM indicated that the samples were covered with a high-quality single-crystal graphene film.[16,17)]

2.2 Fabrication of junction structure

Before constructing the stacked junction, the samples were patterned to limit the square junction region, by employing stencil lithography. The plastic film was patterned using laser machine placed on the sample surface and the samples were subjected to ion etching to remove the uncovered graphene on the SiC substrate. The two samples were stacked in a face-to-face manner as shown in Fig. 1(a). The dark blue region is graphene and light blue region is SiC substrate after graphene removed. Four contact probes with gold sheets as contact materials were placed on the surfaces of the graphene samples. Two electrodes (1 and 2) were connected to sample A and the other two electrodes (A and B) were connected to sample B. Sample A was immersed in DI water for 15 min to form the structured water layer on the graphene surface. The sample A and sample B were stacked each other in the face-to-face manner. A pair of acrylic molds were used for fixing graphene samples. The schematic of the stacked junction is shown in Fig.1(b). The distance of molds was controlled by four screws at corners of molds. The electrical measurements of the junctions were performed by a four-terminal method at room temperature under atmospheric conditions.

3. Results and discussion

3.1 Electrical properties of stacked graphene junction

The current-voltage (*I*-*V*) characteristics of the graphene-graphene direct contact junction

(without tunnel barrier) are shown in Fig.2. Because the results of both two-terminal and four-terminal measurements were linear, it could be inferred that both the graphene-graphene and graphene-probe junctions established ohmic contacts[18,19)]. The resistance of the graphene-graphene junction was 30.1 kΩ and the graphene-probe junction was 135.45 kΩ. After DI water treatment of one sample (sample A), the zero-bias resistance of the stacked junction increased drastically to approximately 1.3 GΩ. As shown in Fig.3(a), non-linear *I-V* characteristics were observed. The semi-log plot of the *I-V* characteristics, shown in Fig.3(b), that the dynamic range of current change reached the sixth order of magnitude. The d*I*/dV curve of the stacked graphene junction with water layer barrier is shown in Fig.3(c). The conductance is constant around zero voltage. This result suggests that the DT phenomenon may be observed in the low-electric-field region and will be discussed later.

3.2 Tunneling phenomena in stacked graphene junction with water layer barrier

Very thin two-dimensional materials as barrier in stacked graphene junctions were reported recently[20,21)], which make it possible to observe DT and FNT phenomenon. In the low-electric-field regime, the carriers in graphene can be transferred to the other graphene sample through the tunneling barrier by DT, which is shown in the schematic of Fig.4(a). When the bias voltage applied to the junction barrier is large, the shape of the barrier-region potential becomes triangular, and the tunneling mechanism changes from DT to FNT, as shown in Fig.4(b).[22,23)] Figure 5(a) shows the topographic SPM image of the graphene surface after DI water treatment. The step-terrace structures originating from the SiC crystallography can be observed. The lower terraces are covered by bilayer graphene with island-like structures. In the upper terraces, monolayer graphene is dominant. In the monolayer graphene region, hole structures are observed. The depth of the hole corresponds to be thickness of the structured water layer formed by DI water treatment. The measured thickness of the water layer is approximately 0.46 nm, as shown in the cross-sectional profile of Fig. 5(b).

3.2.1 Direct tunneling

In the DT regime, the tunneling current is proportional to the bias voltage, as expressed in the following equation,[24,25)]

$$I \propto V\, exp\left[\frac{-2d\sqrt{2m_e\Phi}}{\hbar}\right], \quad (1)$$

where d is the barrier width, Φ is the work function, $\hbar$ is the reduced Planck's constant, and m_e is the electron effective mass. As shown in Fig. 3(c), the electrical conductance around zero bias has a constant value that conforms to the I-V proportionality relationship in Eq. (1). This result indicates that the structured water layer on graphene is thin enough to observe the DT phenomenon clearly.

3.2.2 Fowler-Nordheim tunneling

On increasing the bias voltage, the tunneling phenomenon changes from DT to FNT. As shown in the FN plot of Fig. 6, linear regions appear at high electric fields for both the negative and positive biased regions. The tunneling current in the FNT regime can be expressed as:[24-27)]

$$I \propto V^2\, exp\left[\frac{-4d\sqrt{2m_e\Phi^3}}{3\hbar qV}\right], \quad (2)$$

It is possible to estimate the thickness of tunneling barrier (d) from the slope of the FN plot, which corresponds to the exponential component of Eq. (2). To evaluate d, the work function value Φ, and the effective mass of the electron m_e should be assumed. Because the graphene on the SiC substrate is strongly electron doped, the work function of our graphene sample will be smaller than that of undoped graphene[28)]. The Fermi level shift, ΔE_F can be expressed by the following equation: [2,29)]

$$\Delta E_F = \hbar v_F \sqrt{\pi n}. \quad (3)$$

where n is the carrier density of graphene and v_F is the Fermi velocity, which is approximately 1.1×10^8 cm/s.[30)] The carrier concentration of sample B is measured to be 6.04×10^{12} cm^{-2}, by Hall measurement. By assuming the work function of pristine graphene to be 4.56 eV,[28)] the work function of sample B can be estimated to be 4.25 eV. The ratio of effective mass, m_e/m_0 is assumed to be 0.42.[26)] The thickness of the tunneling

barrier d, in the FNT regime can be calculated as 0.28 nm from the experimental slope in Fig. 6(a). The barrier thickness estimated from the FNT equation is smaller than the measured thickness of the water layer in Fig. 5(b), which corresponds to a few layers of water molecules.[31)] The thickness of water layer before direct bonding was almost constant to be 0.46 nm as shown in Fig.5. After bonding, the thickness of water layer should be not uniform because of the roughness of the sample surface. The electron emission dominantly occurred at the thinner barrier region. In this case, the evaluated thickness of structured water layer is 0.28 nm which is smaller than the average thickness.

As shown in Fig.3(a), asymmetric behavior is observed in the I-V curve. The cause of this asymmetry can be attributed to the work function difference between samples A and B. The difference of current in the backward (negativity bias) region and the forward (positive bias) region (Fig. 3(a)) reflects on the difference of slop in FN-plot (Fig. 6). The work function of sample A after water treated will be slightly larger than sample B, because the slope of Fig.6(b) is smaller than that of Fig. 6(a). The estimated value of the work function for sample A after water treated is 4.51 eV which was calculated from FN-plot of Fig.6(b). The sheet carrier density of sample A by using the estimated work function is 1.73×10^{11} cm^{-2}. The estimated carrier density of sample A decreases owing to the p-type doping of 5.31×10^{12} cm^{-2} caused by the DI water treatment. It is known that the structured water layer formed by the DI water treatment acts as a p-type dopant[15)]. Thus, the asymmetry in the I-V characteristics is attributed to the work-function difference caused by the DI water treatment. The doping effect for sample B (without DI treatment) by contacting water layer is smaller than that of structured water layer for sample A.

This work presents the first ever observation of the tunneling phenomenon through a water barrier in stacked graphene junctions, which is significant for applications in resonant tunneling and terahertz emission. The structured water on graphene at the junction was thin enough (<0.5nm, a few layer of water molecule) to allow the observation of DT and was stable in high electric field of FNT regime. Tunneling resistances of direct tunnel region were almost constant for various bias voltages and were

stable for 80 hours at least. Further experimental will be required for confirming the stability and reproducibility of structured water insulated layer. At this point, maximum device power (6 μW) is so small because of the small contact area. Enhancement of power should also be required for the practical device.

4. Conclusions

In conclusion, a sandwich structure of vertically stacked graphene junctions with a water barrier was constructed successfully through simple water treatment. By analyzing the *I*-*V* characteristics, the zero-bias resistance was found to be approximately 1.3 GΩ. Both DT and FNT phenomena were observed, which proved that the water barrier was thin enough. From the experimental FNT plot and SPM data, the thickness of the junction water barrier was estimated to be below 0.5 nm.

References

1) K. S. Novoselov, A. K. Geim1, S. V. Morozov, D. Jiang, Y. Zhang, S. V. Dubonos, I. V. Grigorieva, A. A. Firsov, Science. **306**, 666 (2004).
2) K. S. Novoselov, A. K. Geim, S. V. Morozov, D. Jiang, M. I. Katsnelson, I. V. Grigorieva, S. V. Dubonos, and A. A. Firsov, Nature. **438**, 197(2005).
3) Y. Feng, D. J. Trainer and K. Chen, J. Phys. D: Appl. Phys. **50**, 155101 (2017).
4) V. Ryzhii, A. A. Dubinov, V. Y. Aleshkin, M. Ryzhii, and T. Otsuji, Appl. Phys. Lett. **103**, 163507 (2013).
5) A. A. Dubinov, V. Ya. Aleshkin, M. Ryzhii, T. Otsuji, and V. Ryzhii, Appl. Phys. Express. **2**, 092301 (2009).
6) D. Yadav, S. B. Tombet, T. Watanabe, S. Arnold, V. Ryzhii, and T. Otsuji. 2D Mater. **3**, 045009 (2016).
7) L. Britnell, R. V. Gorbachev, A. K. Geim, L. A. Ponomarenko, A. Mishchenko, M. T. Greenaway, T. M. Fromhold, K. S. Novoselov, and L. Eaves, Nat. Commun. **4**, 1794 (2013).
8) L. Britnell, R. V. Gorbachev, R. Jalil, B. D. Belle, F. Schedin, A. Mishchenko, T. Georgiou, M. I. Katsnelson, L. Eaves, S. V. Morozov, N. M. R. Peres, J. Leist, A. K. Geim, K. S. Novoselov, and L. A. Ponomarenko, Science **335**, 947 (2012).
9) M. P. Levendorf, C. J. Kim, L. Brown, P. Y. Huang, R.W. Havener, D. A. Muller, and J. Park, Nature. **488**, 627 (2012).
10) G. H. Lee, Y. J. Yu, C. Lee, C. Dean, K. L. Shepard, P. Kim, and J. Hone, Appl. Phys. Lett. **99**, 243114 (2011).
11) M. V. Kamalakar, A. Dankert, J. Bergsten, T. Ive, and S. P. Dash, Sci. Rep. **4**, 6146 (2014).
12) J. A. Leon, N. C. Mamani, A. Rahim, L. E. Gomez, M. A. P. da Silva, and G. M. Gusev, Graphene. **3**, 25 (2014).
13) F. Amet, J. R. Williams, A. G. F. Garcia, M. Yankowitz, K. Watanabe, T. Taniguchi,

and D. Goldhaber-Gordon, Phys. Rev. B. **85**, 073405 (2012).

14) W. J. Yu, Z. Li, H. Zhou, Y. Chen, Y. Wang, Y. Huang, and X. Duan, Nat. Mater. **12**, 246 (2013).
15) M. Kitaoka, T. Nagahama, K. Nakamura, T. Aritsuki, K. Takashima, Y. Ohno, and M. Nagase, Jpn. J. Appl. Phys. **56**, 085102 (2017).
16) T. Aritsuki, T. Nakashima, K. Kobayashi, Y. Ohno, and M. Nagase, Jpn. J. Appl. Phys. **55**, 06GF03 (2016).
17) K. Kobayashi, S. Tanabe, T. Tao, T. Okumura, T. Nakashima, T. Aritsuki, R. Soko, and M. Nagase, Appl. Phys. Express. **8**, 036602 (2015).
18) M. Nagase, H. Hibino, H. Kageshima, and H. Yamaguchi, Appl. Phys. Express. **3**, 045101 (2010).
19) M. Nagase, H. Hibino, H. Kageshima, and H. Yamaguchi, Appl. Phys. Express. **6**, 055101 (2013).
20) D. Chu, Y. H. Lee, and E. K. Kim, Sci. Adv. **3**, e1602726 (2017).
21) S. M. Kim, A. Hsu, P. T. Araujo, Y. H. Lee, T. Palacios, M. Dresselhaus, J. C. Idrobo, K. K. Kim, and J. Kong, Nano. Lett. **13**, 3 (2013).
22) V. Garcia and M. Bibes, Nat. Commun. **5**, 4289 (2014).
23) J. Gaskell, L. Eaves, K. S. Novoselov, A. Mishchenko, A. K. Geim, T. M. Fromhold, and M. T. Greenaway, Appl. Phys. Lett. 1**07**, 103105 (2015).
24) J. M. Beebe, B. Kim, J. W. Gadzuk, C. D. Frisbie, and J. G. Kushmerick, Phys. Rev. Lett. **97**, 026801 (2006).
25) J. G. Simmons, J. Appl. Phys. **34**, 1793 (1963).
26) R. Waters and B. Van Zeghbroeck, Appl. Phys. Lett. **73**, 3692 (1998).
27) J. W. Gadzuk and E. W. Plummer, Rev. Mod. Phys. **45**, 487 (1973).
28) R. Yan, Q. Zhang, W. Li, I. Calizo, T. Shen, C. A. Richter, A. R. Hight-Walker, X. Liang, A. Seabaugh, D. Jena, H. G. Xing, D. J. Gundlach, and N. V. Nguyen. Appl. Phys. Lett. **101**, 022105 (2012).
29) D. Ziegler, P. Gava, J. Guttinger, F. Molitor, L. Wirtz, M. Lazzeri, A. M. Saitta, A.

Stemmer, F. Mauri, and C. Stampfer, Phys. Rev. B **83**, 235434 (2011).

30) J. Horng, C. Chen, B. Geng, C. Girit, Y. Zhang, Z. Hao, H. A. Bechtel, M. Martin, A. Zettl, M. F. Crommie, Y. R. Shen, and F. Wang, Phys. Rev. B. **83**, 165113 (2011).

31) L. Cheng, P. Fenter, K. L. Nagy, M. L. Schlegel, and N. C. Sturchio, Phys. Rev. Lett. **87**, 156103 (2001).

Figure Captions

Fig. 1. (Color online) Schematic of graphene/ water barrier/ graphene tunnel junction. (a) Structure charts of tunnel junction for ion-beam sputter treated graphene samples. (b) Cross sectional schematic of water layer barrier junction. Water layer covers graphene surface and metal probes are used for measurement.

Fig. 2. (Color online) Current-voltage (*I-V*) characteristic curve of junction under different voltages at room temperature. The curve is for a graphene-graphene contact junction without water barrier (before water treatment). Both two-terminal and four-terminal measurements show linear characteristics, which indicates that this junction without water barrier is an ohmic contact junction.

Fig. 3. (Color online) (a) *I-V* Characteristics of graphene/ water barrier/ graphene tunnel junction. A non-linear curve is observed after introducing a water barrier to the junction. (b) Semi-log plot of this graphene/ water barrier/ graphene tunnel junction. (c) Differential conductance (dI/dV) curve of vertically stacked graphene junction with water barrier.

Fig. 4. (Color online) Energy band diagrams of the vertically stacked graphene tunnel junction: (a) Direct tunneling (DT). (b) Fowler-Nordheim tunneling (FNT).

Fig. 5. (Color online) (a) Topographic image of graphene surface observed by SPM. (b) Average step height of graphene surface after water treatment (line area). The thickness of water layer is the difference between graphene surface and water layer, which is 0.46 nm depending on the SPM result.

Fig. 6. (Color online) (a) Forward fit linear curve for Fowler-Nordheim (FN) plot. (b) Backward fit linear curve for FN plot. Both FNT and DT are observed in these FN plots.

Fig.1. (Color Online)

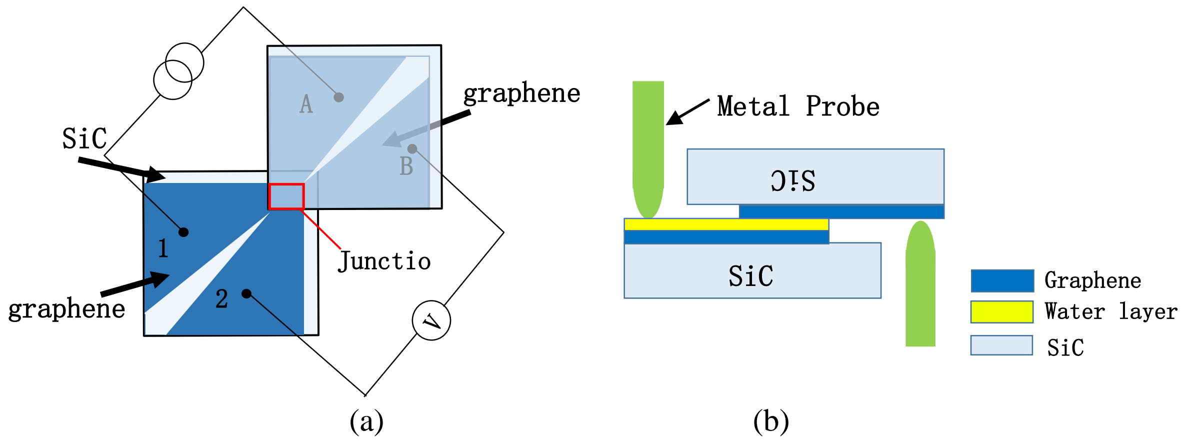

Fig.2. (Color Online)

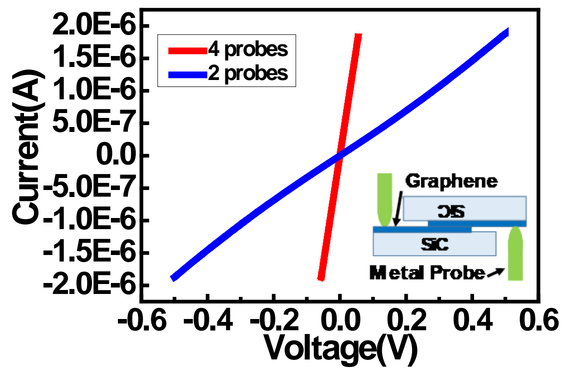

Fig.3. (Color Online)

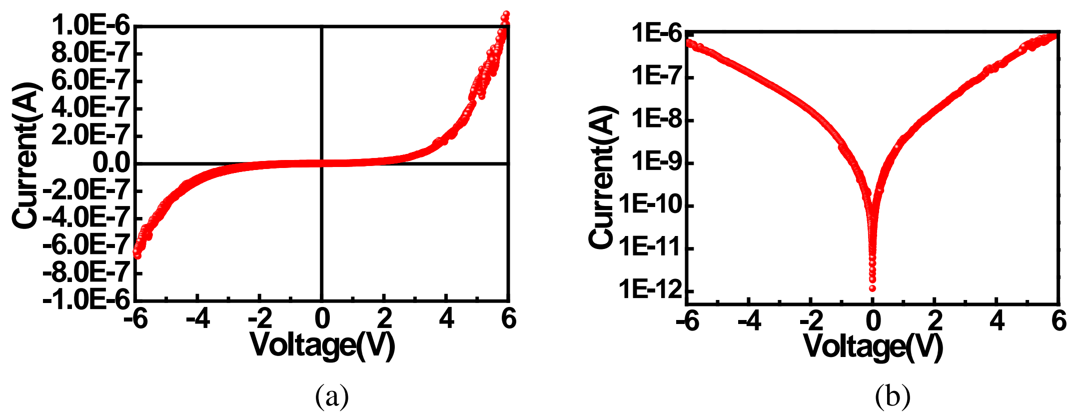

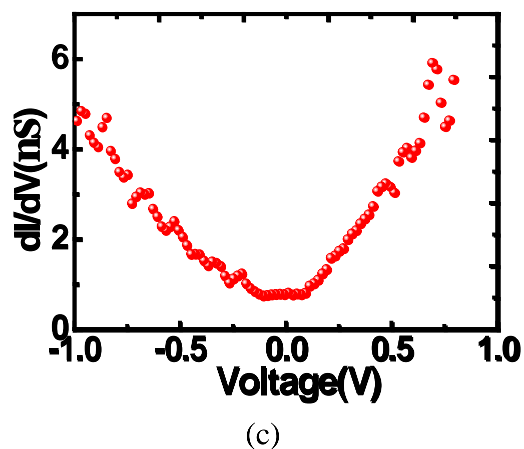

(c)

Fig.4. (Color Online)

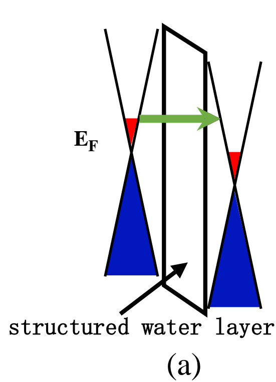

(a)

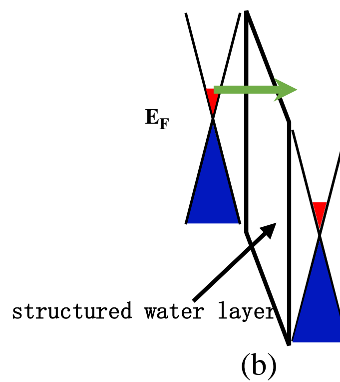

(b)

Fig.5. (Color Online)

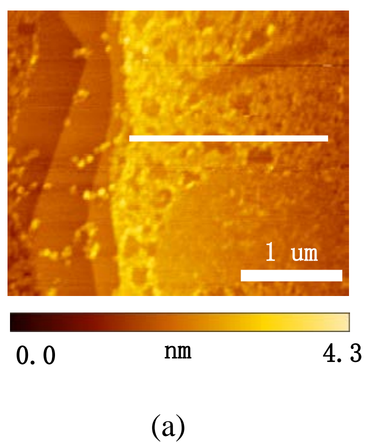

(a)

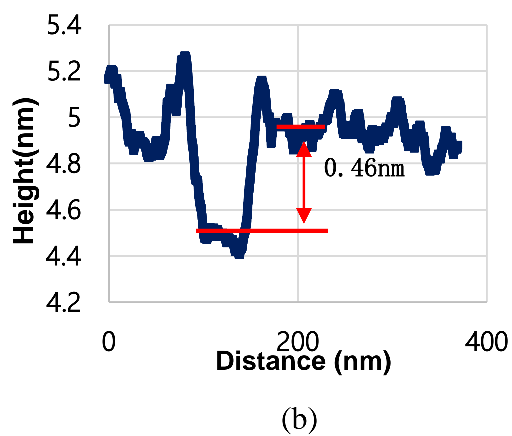

(b)

Fig.6. (Color Online)

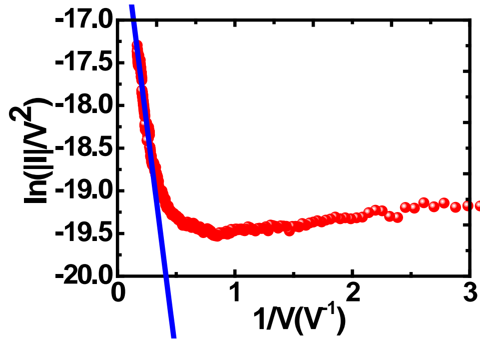

(a)

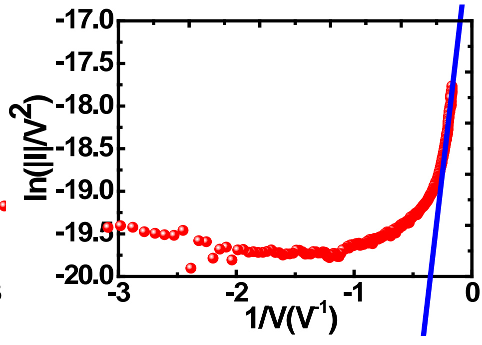

(b)